

# Optimal car-following control for intelligent vehicles using online road-slope approximation method

Hongqing CHU<sup>1</sup>, Lulu GUO<sup>2</sup>, Hong CHEN<sup>1,3</sup> & Bingzhao GAO<sup>1\*</sup><sup>1</sup>State Key Laboratory of Automotive Simulation and Control, Jilin University, Changchun 130022, China;<sup>2</sup>Center for Cyber-Physical systems, University of Georgia, Georgia 30602, USA;<sup>3</sup>Clean Energy Automotive Engineering Center, Tongji University, Shanghai 201804, China

Received 20 May 2019/Revised 6 November 2019/Accepted 26 December 2019/Published online 15 July 2020

**Abstract** The design of a car-following control system is a multiobjective optimization problem that involves issues in rider safety, ride comfort, and fuel economy. This study proposes a hierarchical design of optimal car-following control where the system is intuitively split into two subsystems with different dynamic properties. Specifically, the high-level subsystem is a linear car-following system with a measurable disturbance of the preceding vehicle's acceleration, while the low-level subsystem is a nonlinear acceleration-tracking system with an unmeasurable road slope. In the design of optimal car-following control, the measurable disturbance of the preceding vehicle's acceleration is considered from a theoretical perspective, and the unmeasurable road slope is estimated by a novel engineering-oriented approximation method to reduce the influence of driveline oscillation. The performance of the proposed optimal control scheme is evaluated through simulation and real-vehicle experiments, which show that the proposed control algorithm provides a satisfactory road-slope approximation accuracy and that the car-following performance of the proposed optimal control system is better than that of a factory-installed adaptive cruise controller.

**Keywords** car-following control, road-slope approximation, hierarchical design, linear quadratic regulator, intelligent vehicle

**Citation** Chu H Q, Guo L L, Chen H, et al. Optimal car-following control for intelligent vehicles using online road-slope approximation method. *Sci China Inf Sci*, 2021, 64(1): 112201, <https://doi.org/10.1007/s11432-019-2756-3>

## 1 Introduction

With significant developments in the field of intelligent vehicle technologies, an increased number of advanced driver-assistance systems (ADASs) have been added to vehicles. The longitudinal car-following control system, which is developed to relieve drivers from operating either on the accelerator or the brake pedal, is among the fastest-growing ADAS technologies. The design of a car-following control system is a multiobjective optimization problem that involves issues in rider safety, ride comfort, and fuel economy.

Numerous control methods have been proposed to design a car-following control system. For instance, Ganji et al. [1] presented a sliding mode controller for a car-following system that applies swarm optimization to tune the controller gains. Nilsson et al. [2] employed polyhedral controller invariant sets to design a correct-by-construction car-following control system. Yi et al. [3] used a linear quadratic regulator (LQR) to derive a car-following controller. Li et al. [4] and Chu et al. [5] developed car-following algorithms under the framework of model predictive control (MPC).

Given that the design of a car-following system is a multiobjective optimization problem, among the aforementioned methods, LQR and MPC are expected to address car-following problems owing to their multiple-criteria decision-making capabilities [3, 6–8]. However, the huge computational burden from finding a numerical solution restricts the application of MPC in real vehicles. To the best of our knowledge, the present LQR formulations do not consider the longitudinal acceleration of the preceding vehicle from a theoretical perspective. For example, in [3, 7, 8], the acceleration of the preceding vehicle is treated as a disturbance and, consequently, the derived control law does not contain this acceleration

\* Corresponding author (email: Gaobz@jlu.edu.cn)

information. From the information utilization perspective, ignoring the acceleration information presents a deficiency because introducing the longitudinal acceleration of surrounding vehicles can help reduce the collision probability and improve the safety of vehicles [9,10]. In reality, the acceleration of the preceding vehicle is readily available to the host vehicle. For instance, the acceleration of the preceding vehicle is estimated by using a Kalman filter [6], while vehicle-to-vehicle (V2V) communication [11] and intervehicle interaction [12] are used to access this type of information.

In implementing a car-following system for passenger vehicles, one key issue relates to how to compensate for the influence of road-slope variations [7]. The road slope can be obtained from an ADAS map according to the vehicle positioning information provided by a global positioning system (GPS) [13]. However, it will involve GPS signal loss and positioning error issues [14]. Given that the road slope cannot be directly measured for a moving vehicle, an alternative way is to estimate the road slope and use a feedforward strategy to attenuate the influence of road-slope variations. Road-slope estimation algorithms are generally classified as acceleration- [15,16], GPS- [17,18], and vehicle-model- [19,20] based algorithms. Unlike the GPS-based estimation algorithm, the acceleration- and vehicle-model-based algorithms require the vehicle speed signal. However, owing to the undamped characteristics of the vehicle driveline, the vehicle speed is accompanied by periodic fluctuations known as driveline oscillations. Jo et al. [15] found that the inertial sensor-based road-slope estimation algorithms suffer from an oscillation problem that deteriorates their estimated performance.

This study proposes a hierarchical design of an optimal car-following control system that is intuitively split into two subsystems with different dynamic properties. On the one hand, the car-following subsystem (high level) is linear with a measurable disturbance, while on the other hand, the acceleration-tracking subsystem (low level) is nonlinear with an unmeasurable road slope. As one of its advantages, this hierarchical structure allows these two subsystems to be designed independently. The car-following control system is designed by using an LQR optimal control method where the dynamics of the low level are taken into account. Meanwhile, the acceleration-tracking control system is designed via a feedforward and feedback approach where an online slope approximation method is incorporated into the feedforward item. The interaction between these two subsystems is guaranteed by the longitudinal acceleration of the vehicle, which is the control reference of the acceleration-tracking control system and the control input of the car-following control system.

The main contributions of this study are summarized as follows. First, compared with other car-following controllers that are designed based on the LQR method, the proposed optimal car-following controller takes the longitudinal acceleration of the preceding vehicle into consideration from a theoretical perspective to improve vehicle safety. Second, in designing the acceleration-tracking control system, a novel engineering-oriented road-slope approximation method that can effectively attenuate the influence of driveline oscillation is proposed. Third, the proposed control scheme is evaluated through simulations and real-vehicle experiments. The experimental results show that the proposed online road-slope approximation method achieves a satisfactory road-slope approximation accuracy (the maximal absolute approximation error is less than  $0.8^\circ$ ) and that the car-following performance of the proposed control scheme is better than that of a factory-installed adaptive cruise controller (ACC).

The rest of this paper is organized as follows. Section 2 presents the system model including the vehicle longitudinal dynamics and the car-following model. Section 3 proposes a hierarchical system architecture and designs high-level and low-level controllers by using different methods. Sections 4 and 5 evaluate the proposed cruise control scheme through simulations and real-vehicle experiments, respectively. Section 6 presents the conclusion.

## 2 System model

### 2.1 Vehicle longitudinal dynamics

The intelligent vehicle under investigation is a production sport-utility vehicle (SUV) driven by a 2.0-L internal combustion engine (ICE) mated to a six-speed automatic transmission (AT). According to Newton's second law, the longitudinal dynamics of the SUV can be modeled as

$$\kappa m_v a_v = \frac{T_w - T_b}{r_w} - \frac{1}{2} C_D A_a \rho v^2 - m_v g (f \cos(\alpha) + \sin(\alpha)), \quad (1)$$

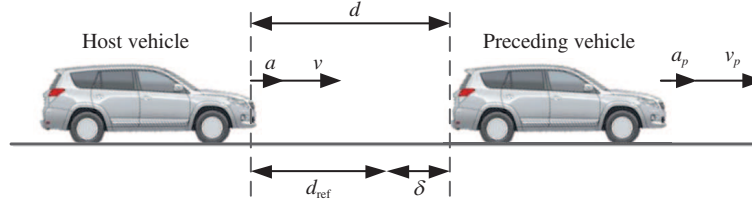


**Figure 1** (Color online) Schematic diagram of a car-following scenario.

where  $m_v$  is the mass of the vehicle,  $a_v$  is the longitudinal acceleration of the vehicle,  $\kappa$  is the lumped rotational inertial coefficient,  $r_w$  is the wheel radius,  $T_w$  is the traction torque,  $T_b$  is the braking torque,  $f$  is the rolling resistance coefficient,  $C_D$  is the aerodynamic drag coefficient,  $A_a$  is the frontal area,  $\rho$  is the air density,  $v$  is the vehicle speed,  $g$  is the gravity constant, and  $\alpha$  is the slope angle.

The traction torque  $T_w$  and braking force  $T_b$  are system inputs and do not work simultaneously. The traction torque  $T_w$  comes from the ICE and is governed by

$$T_w = \begin{cases} \eta_t I_0 I_g T_e, & T_e \geq 0, \\ \frac{I_0 I_g}{\eta_t} T_e, & T_e < 0, \end{cases} \quad (2)$$

where  $I_0$  is the conversion ratio of the final gears,  $\eta_t$  is the mechanical transmission efficiency,  $T_e$  is the engine torque,  $I_g$  is the discrete gear ratio, and  $I_g \in \{I_{g1}, I_{g2}, I_{g3}, I_{g4}, I_{g5}, I_{g6}\}$ . The braking torque  $T_b$ , which is related to brake pressure  $P_b$  and brake system gain  $K_b$  [21], can be formed as

$$T_b = K_b P_b. \quad (3)$$

To describe the dynamics of actuators, the dynamic models of the engine torque and brake pressure are approximated by the following two first-order systems [22]:

$$T_e = \frac{T_e^*}{\tau_{\text{eng}} s + 1}, \quad P_b = \frac{P_b^*}{\tau_{\text{bra}} s + 1}, \quad (4)$$

where  $T_e^*$  and  $\tau_{\text{eng}}$  are the desired torque and time constant of the ICE, while  $P_b^*$  and  $\tau_{\text{bra}}$  are the desired brake pressure and time constant of the brake system, respectively.

## 2.2 Car-following model

A schematic diagram of the car-following scenario is shown in Figure 1. Two state variables, namely, the spacing error  $\delta = d - d_{\text{ref}}$  and relative speed  $\varpi = v_p - v$ , are introduced to describe the longitudinal dynamics between the two vehicles. Here,  $d$  is the intervehicle distance between the preceding and host vehicles,  $v_p$  is the preceding vehicle speed, and  $d_{\text{ref}}$  is the spacing policy of the host vehicle. There are two major spacing policies in the car-following scenario, namely, the fixed desired intervehicle distance and the velocity-dependent spacing policy [23]. In this study, the velocity-dependent spacing policy is used:

$$d_{\text{ref}} = d_0 + \tau v, \quad (5)$$

where  $d_0$  is the desired intervehicle distance when the preceding and host vehicles are at a standstill, and  $\tau$  is the nominal time headway. Therefore, the dynamics of the spacing error and relative speed can be formulated as

$$\dot{\delta} = \varpi - \tau a_v, \quad \dot{\varpi} = a_p - a_v, \quad (6)$$

where  $a_v$  is the longitudinal acceleration of the host vehicle, and  $a_p$  is the longitudinal acceleration of the preceding vehicle. Following the ideas in [6], the longitudinal acceleration dynamics are approximated as follows by a first-order system:

$$\dot{a}_v = -\frac{1}{\tau_i} a_v + \frac{1}{\tau_i} a_{\text{ref}}, \quad (7)$$

where  $\tau_i$  is the acceleration time constant, and  $a_{\text{ref}}$  is the system input of the host vehicle.

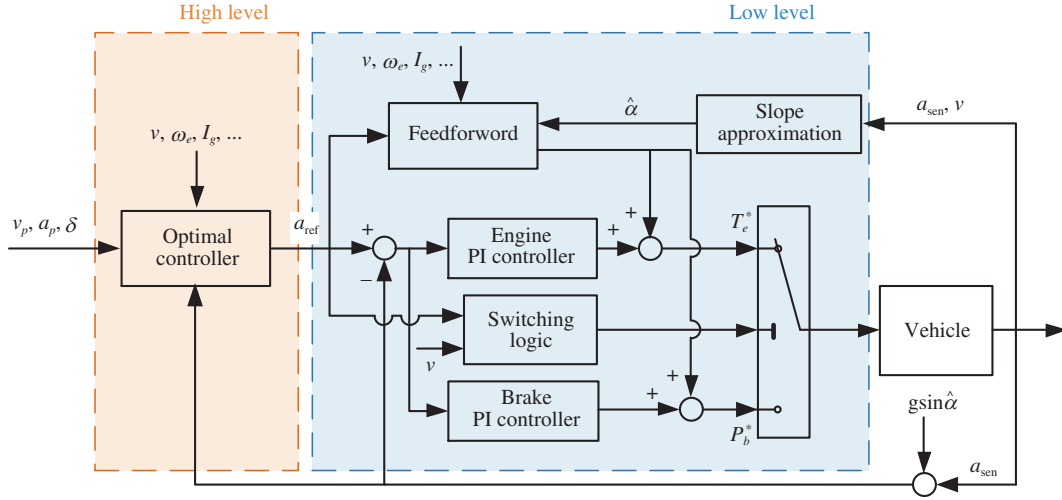


**Figure 2** (Color online) Architecture of the proposed optimal car-following control.

By combining (6) and (7), the continuous-time state-space equation is described by

$$\dot{x} = Fx + G_u u + G_d d, \quad (8)$$

where

$$x = \begin{bmatrix} \delta \\ \varpi \\ a_v \end{bmatrix}, \quad F = \begin{bmatrix} 0 & 1 & -\tau \\ 0 & 0 & -1 \\ 0 & 0 & -\frac{1}{\tau_i} \end{bmatrix}, \quad G_u = \begin{bmatrix} 0 \\ 0 \\ \frac{1}{\tau_i} \end{bmatrix}, \quad G_d = \begin{bmatrix} 0 \\ 1 \\ 0 \end{bmatrix}, \quad u = a_{ref}, \quad d = a_p.$$

For a convenient controller design, the state-space equation of the car-following system is represented by a discrete time system using the zero-order-hold method. Define state vector  $x(k) = [\delta(k) \ \varpi(k) \ a_v(k)]^T$  and control input  $u(k) = a_{ref}(k)$ . Then,

$$x(k+1) = Ax(k) + B_u u(k) + B_d d(k), \quad (9)$$

where

$$A = \begin{bmatrix} 1 & T_s & -T_s \tau \\ 0 & 1 & -T_s \\ 0 & 0 & 1 - \frac{T_s}{\tau_i} \end{bmatrix}, \quad B_u = \begin{bmatrix} 0 \\ 0 \\ \frac{T_s}{\tau_i} \end{bmatrix}, \quad B_d = \begin{bmatrix} 0 \\ T_s \\ 0 \end{bmatrix}, \quad d(k) = a_p(k),$$

and  $T_s$  is the sampling time. Variable  $a_p(k)$  can be derived from the preceding vehicle speed by filtering algorithms or via V2V. Spacing error  $\delta$  and relative speed  $\varpi$  can be directly measured. The longitudinal acceleration of the host vehicle  $a_v$  can be obtained from the accelerometer by subtracting the effect of the road slope, namely,  $a_v = a_{sen} - g \sin \alpha$ , where  $a_{sen}$  is the measured vehicle acceleration.

### 3 Hierarchical design of car-following controller

#### 3.1 System architecture

The proposed optimal car-following control is separated into a high-level controller and a low-level controller, as shown in Figure 2. The high-level controller provides an acceleration reference by using an optimal controller. The tracking of this reference signal is ensured by the lower-level controller, which determines the engine torque and brake pressure. This separation is necessary because these two control systems have different dynamic properties. Specifically, the car-following model is linear with a measurable disturbance, while the vehicle longitudinal model is nonlinear with an unmeasurable road slope.

This hierarchical structure allows these two control systems to be designed independently, thereby helping reduce the design complexity.

The high- and low-level controllers are designed by using the LQR and feedforward-feedback methods, respectively. The LQR method takes ride comfort and fuel economy into account and provides humanlike driving actions. Meanwhile, the feedforward-feedback method is used to offer input references for different actuators. Given the different response characteristics of the ICE and brake system, two proportional-integral (PI) controllers with different control gains are used in the error feedback items, and a switching logic is introduced to schedule these two actuators. Owing to introducing an online road-slope approximation method into the feedforward item, the feedback item becomes a small deviation adjustment, which is conducive to improving the tracking performance.

### 3.2 Optimal control design

#### 3.2.1 Quadratic optimal control problem

This subsection presents the formulation of the optimal problem for the car-following scenario. Unlike the present optimal controllers that do not take the longitudinal acceleration of the preceding vehicle into consideration as in [3, 7, 8], the acceleration of the preceding vehicle is used to derive an optimal car-following controller from a theoretical perspective. Taking into account ride comfort and fuel economy, the performance index to be minimized is formulated as

$$J = \frac{1}{2} \sum_{k=0}^{\infty} (x^T(k)Qx(k) + u^T(k)Ru(k)), \quad (10)$$

where  $Q$  is a  $(3 \times 3)$  symmetric and positive-semidefinite matrix, and  $R$  is a  $(1 \times 1)$  nonnegative scalar.

Defining  $Q$  and  $R$  as

$$Q = \begin{bmatrix} q_{11} & 0 & 0 \\ 0 & q_{22} & q_{23} \\ 0 & q_{23} & 0 \end{bmatrix}, \quad R = r,$$

the performance index  $J$  becomes

$$\frac{1}{2} \sum_{k=0}^{\infty} (q_{11}\delta^2(k) + q_{22}\varpi^2(k) + 2q_{23}\varpi(k)a_v(k) + ra_{\text{ref}}^2(k)). \quad (11)$$

Clearly,

- the penalty item  $q_{11}\delta^2(k) + q_{22}\varpi^2(k)$  obtains a desired car-following characteristic (i.e., to force spacing error  $\delta$  and relative speed  $\varpi$  to converge to small values);
- the penalty item  $2q_{23}\varpi(k)a_v(k)$  minimizes the fuel consumption; and
- the penalty item  $ra_{\text{ref}}^2(k)$  improves the ride comfort by penalizing the acceleration magnitude.

For a constant-mass system, variables  $a_v(k)$  and  $\varpi(k)$  correspond to the applied force and the system speed, respectively. The penalty item  $2q_{23}\varpi(k)a_v(k)$  is related to the system power. Therefore, penalizing this item is related to minimizing the fuel consumption. After careful consideration, the penalty items  $q_{11}\delta^2(k) + q_{22}\varpi^2(k)$  and  $ra_{\text{ref}}^2(k)$  are found to be contradicting. A perfect tracking of the spacing error  $\delta$  and relative speed  $\varpi$  is often achieved at the expense of fluctuation of the longitudinal acceleration. Therefore, the choice of weighting coefficients is a trade-off.

#### 3.2.2 Solution

Following the ideas in [24, 25], we introduce the Hamilton function as follows:

$$H(k) = \frac{1}{2}(x^T(k)Qx(k) + u^T(k)Ru(k)) + \lambda^T(k+1)(Ax(k) + B_u u(k) + B_d d(k)), \quad (12)$$

where  $\lambda(k+1) \in \mathbb{R}^{3 \times 1}$  is the Lagrange multiplier. To minimize the function  $H(k)$ , the optimal solution must satisfy the following conditions [24]:

$$Ru(k) + B_u^T \lambda(k+1) = 0, \quad (13a)$$

$$Qx(k) + A^T\lambda(k+1) - \lambda(k) = 0. \quad (13b)$$

By solving (13a) for  $u(k)$  and by noting that  $R^{-1}$  exists, we obtain

$$u(k) = -R^{-1}B_u^T\lambda(k+1). \quad (14)$$

Choosing the covector  $\lambda(k)$  as follows:

$$\lambda(k) = Px(k) + hd(k), \quad (15)$$

system disturbance  $d(k)$  (the acceleration of the preceding vehicle) can be explicitly included in the control law (14), where  $P \in \mathbb{R}^{3 \times 3}$  and  $h \in \mathbb{R}^{3 \times 1}$  are the matrices to be determined. Such a choice makes the following derivation different from the classical LQR approach.

By referring to (14), (15) and (13b), the optimal control law is given by

$$u(k) = K_x x(k) + K_d d(k) = -R^{-1}B_u^T(A^T)^{-1}(P - Q)x(k) - R^{-1}B_u^T(A^T)^{-1}hd(k), \quad (16)$$

where  $K_x \in \mathbb{R}^{1 \times 3}$  and  $K_d \in \mathbb{R}$  are the controller gains. Obviously, the longitudinal acceleration of the preceding vehicle  $a_p(k)$  is explicitly included in the optimal control law.

In the optimal control law (16), matrices  $P$  and  $h$  are to be determined, and we now turn our attention to finding them. Substituting (15) and (14) into (9) results in

$$\begin{aligned} x(k+1) &= Ax(k) - B_u R^{-1} B_u^T (Px(k+1) + hd(k+1)) + B_d d(k) \\ &= (I + B_u R^{-1} B_u^T P)^{-1} Ax(k) + (I + B_u R^{-1} B_u^T P)^{-1} (B_d d(k) - B_u R^{-1} B_u^T hd(k+1)). \end{aligned} \quad (17)$$

Substituting (15) into (13b) yields

$$\begin{aligned} Qx(k) + A^T(Px(k+1) + hd(k+1)) - (Px(k) + hd(k)) \\ = (Q - P)x(k) + A^T Px(k+1) + A^T hd(k+1) - hd(k) = 0, \end{aligned} \quad (18)$$

and substituting (17) into (18) yields

$$\begin{aligned} (Q - P + A^T(P^{-1} + B_u R^{-1} B_u^T)^{-1} A)x(k) \\ + A^T(P^{-1} + B_u R^{-1} B_u^T)^{-1} (B_d d(k) - B_u R^{-1} B_u^T hd(k+1)) - hd(k) + A^T hd(k+1) = 0. \end{aligned} \quad (19)$$

Eq. (19) must hold for all  $x(k)$ . We have the following Riccati equation:

$$Q - P + A^T(P^{-1} + B_u R^{-1} B_u^T)^{-1} A = 0. \quad (20)$$

By using the relationship of  $(P^{-1} + B_u R^{-1} B_u^T)(P - PB_u(R + B_u^T PB_u)^{-1} B_u^T P) = I$ , the Riccati (20) can be modified to

$$P = A^T P A - A^T P B_u (R + B_u^T P B_u)^{-1} B_u^T P A + Q. \quad (21)$$

If  $d(k+1)$  can be obtained at step  $k$ , then we can find the solution of  $h$  from (18). Given that the future information  $d(k+1)$  is usually not known at step  $k$ , we assume that  $d(k+1) = d(k)$ . Therefore, Eq. (19) becomes

$$(A^T(P^{-1} + B_u R^{-1} B_u^T)^{-1} (B_d - B_u R^{-1} B_u^T h) - h + A^T h)d(k) = 0. \quad (22)$$

In this case, the explicit solution of  $h$  is obtained as

$$h = -(A^T - I - A^T(P^{-1} + B_u R^{-1} B_u^T)^{-1} B_u R^{-1} B_u^T)^{-1} A^T(P^{-1} + B_u R^{-1} B_u^T)^{-1} B_d. \quad (23)$$

Note that the derivation from (19) to (23) can be obtained because (13a) and (13b) are necessity conditions of the optimal solution. We only need to find a solution that satisfies these conditions.

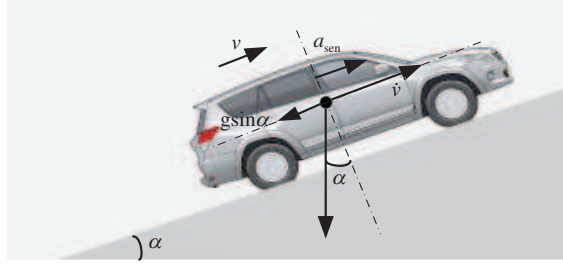


Figure 3 (Color online) Sketch of the longitudinal acceleration in slope.

### 3.3 Tracking control design based on online road-slope approximation method

The low-level controller aims to track the acceleration reference as accurately as possible. As shown in Figure 2, the controller contains feedforward and feedback parts. An online road-slope approximation method is added to the feedforward model to attenuate the influence of the slope angle.

By defining  $F_{\text{req}} = \kappa m_v a_{\text{ref}} + \frac{1}{2} C_D A_a \rho v^2 + m_v g (f \cos(\alpha) + \sin(\alpha))$  and  $e = a_{\text{ref}} - a_v$ , the control law is obtained as

$$\begin{aligned} \text{Traction control} &\Rightarrow \begin{cases} T_e^* = F_{\text{req}} \frac{r_w}{\eta_t I_0 I_g} + k_{p0}(e)e + k_{i0}(e) \int e dt, \\ P_b^* = 0, \end{cases} \\ \text{Brake control} &\Rightarrow \begin{cases} T_e^* = 0, \\ P_b^* = -F_{\text{req}} \frac{r_w}{K_b} + k_{p1}(e)e + k_{i1}(e) \int e dt, \end{cases} \end{aligned} \quad (24)$$

where  $k_{p0}(e)$  and  $k_{i0}(e)$  are the controller gains of the engine torque, and  $k_{p1}(e)$  and  $k_{i1}(e)$  are the controller gains of the brake pressure. Given that these controller gains are error dependent, the feedback parts are two gain-scheduled PI controllers. The choice of controller gains is a trade-off between a fast convergence of the tracking error and a small effect of introducing measurement noise. When the tracking error is large, a large controller gain is required to guarantee a fast convergence rate. By contrast, when the tracking error is small, a small controller gain is sufficient to guarantee a good tracking performance owing to less noise introduction. The different dynamic responses of the engine and brake systems make the controller gains different.

The slope angle  $\alpha$  is substituted by its approximation in the implementation of the control law (24). Given that the road slope is slow time-varying (assume  $\alpha(k) = \alpha(k-1)$ ), the slope angle of the previous step  $\alpha(k-1)$  is used to calculate  $F_{\text{req}}$ . In addition, the calculation of  $a_v = a_{\text{sen}} - g \sin \alpha$  uses the road-slope approximation of the previous step, i.e.,  $a_v(k) = a_{\text{sen}}(k) - g \sin \alpha(k-1)$ .

### 3.4 Online road-slope approximation method

The road slope is estimated online by an approximation method for two reasons. First, the influence of the slope angle on the tracking performance is greater than that of other vehicle parameters. Among parameters  $m_v$ ,  $\kappa$ ,  $r_w$ ,  $f$ ,  $C_D$ ,  $A_a$ ,  $\rho$ ,  $g$ , and  $\alpha$ , the slope angle  $\alpha$  varies along with the vehicle location and is a state-dependent variable. Compared to other parameters that do not change, the state-dependent variable  $\alpha$  has a large impact on the acceleration tracking performance. Therefore, the slope angle is considered as a major external disturbance. Second, the proposed slope approximation method is simple (without complex matrix operations) yet practical. It can be seen from Figure 2 that the feedforward model contains the approximation of the road slope. The approximation accuracy of the road slope affects the accuracy of the feedforward model. An accurate feedforward model makes the gains of the feedback part smaller, and less noise of the acceleration sensor is introduced into the tracking controller. Consequently, a good tracking performance can be improved by less noise introduction.

As shown in Figure 3, when a vehicle is running on a slope, the relationship between the measured vehicle acceleration  $a_{\text{sen}}$  and the differential of the velocity  $\dot{v}$  is

$$g \sin \alpha = \dot{v} - a_{\text{sen}}. \quad (25)$$

This relationship illustrates why the accelerometer cannot directly measure the longitudinal acceleration.

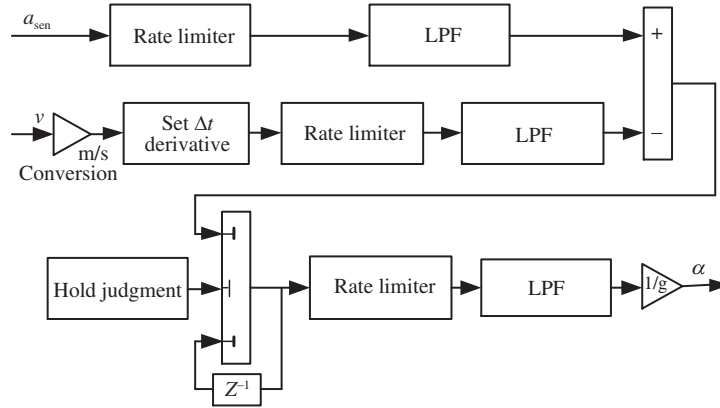


Figure 4 Block diagram of the road-slope approximation method.

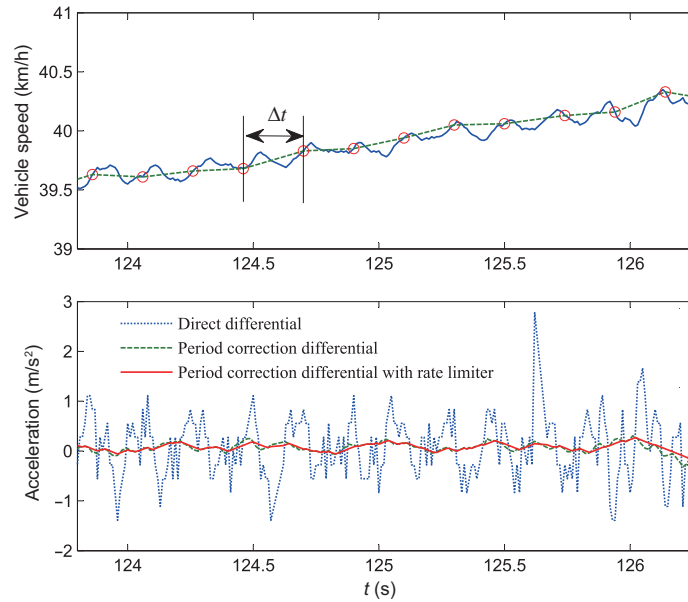


Figure 5 (Color online) Acceleration obtained from the signal of vehicle speed.

By solving (25), the slope angle is calculated as

$$\alpha \approx \sin \alpha = \frac{\dot{v} - a_{sen}}{g}. \tag{26}$$

An engineering-oriented road-slope approximation method is proposed based on (26), as shown in Figure 4. This approximation method comprises four parts, namely, the vehicle speed differential, rate limiter, low-pass filter (LPF), and hold judgment. The rate limiter is introduced to limit the first derivative of the signal and to subsequently avoid an abnormal rate of change, the LPF filters out high-frequency noise, and the hold judgment maintains the value of the last sample when the road-slope approximation method can no longer be applied.

A period correction operation is used in the vehicle speed differential to reduce the influence of the driveline oscillation. A sample longitudinal acceleration obtained by using the proposed differential correction operation (Figure 4) is shown in Figure 5. The vehicle speed profile is obtained from experimental data. As shown in Figure 5, the vehicle speed fluctuates at a specific oscillation frequency. Based on the oscillation frequency, we set the differential time interval  $\Delta t$  of the speed signal and then let the differential signal pass through a rate limiter and an LPF to obtain a usable longitudinal acceleration. As seen in Figure 5, the influence of the driveline oscillation on the differential value can be effectively attenuated.

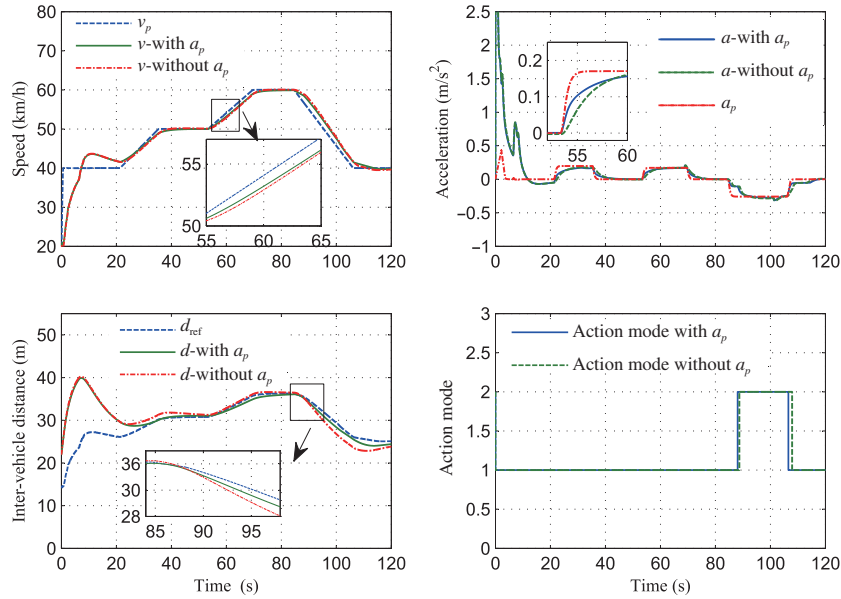


**Figure 6** (Color online) Comparison of the optimal controller with and without the acceleration signal of the preceding vehicle (action mode: 1-traction control; 2-brake control).

## 4 Simulation results

The goal of the following simulation is to show the effectiveness of the proposed car-following control scheme. The model of an SUV is constructed by using the commercial software Carsim, while the proposed control scheme is established in MATLAB/Simulink. In the simulation, the speed of the preceding vehicle and the intervehicle distance are captured by virtual sensors, and the longitudinal acceleration of the preceding vehicle is derived from the speed signal. The simulation studies can be divided into two parts, namely, comparing the results with and without the acceleration signal and evaluating the car-following performance for cut-in and cut-out scenarios.

### 4.1 Comparison of results with and without acceleration signal of preceding vehicle

To evaluate the car-following performance after introducing the longitudinal acceleration of the preceding vehicle, we compare the performances of the proposed optimal controller with and without the acceleration signal under the same velocity profile of the preceding vehicle. Gains in the low-level controller are consistent for the comparison simulation. The predefined velocity profile includes acceleration, constant speed, and deceleration conditions. The comparison results are shown in Figure 6, which reveals that the proposed optimal controller provides an acceptable desired acceleration of less than  $2.5 \text{ m/s}^2$ , thereby showing a satisfactory car-following performance. The enlarged view of this figure shows that compared with the optimal controller without the acceleration signal of the preceding vehicle, the proposed optimal controller provides a relatively fast control input regardless of acceleration or deceleration, and the intervehicle distance can quickly reach a steady state. When the preceding vehicle decelerates, the braking action of the host vehicle with the acceleration information of the preceding vehicle starts earlier than that without the acceleration information, thereby helping improve vehicle safety. In summation, introducing the acceleration signal of the preceding vehicle improves the car-following performance.

### 4.2 Car-following performance for cut-in and cut-out scenarios

We mimic cut-in and cut-out scenarios to comprehensively verify the proposed optimal car-following controller. The entire scene is designed as follows. The host vehicle follows a preceding vehicle in one lane as a vehicle in the adjacent lane suddenly inserts itself between these two vehicles. After a while, the cut-in vehicle drives out of its position between the two vehicles.

In these scenarios, the intervehicle distance rapidly decreases owing to the sudden appearance of the cut-in vehicle for cut-in conditions, and the intervehicle distance also quickly increases for cut-out conditions. The sudden changes in the intervehicle distance can be used to verify the performance of the proposed

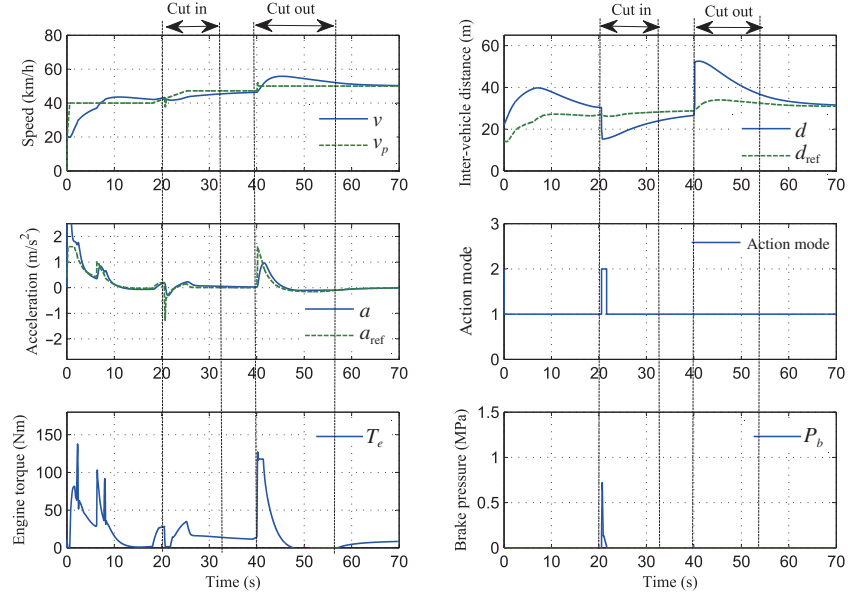


**Figure 7** (Color online) Simulation results of the proposed control scheme for cut-in and cut-out scenarios (action mode: 1-traction control; 2-brake control).

controller. The simulation results in these scenarios are shown in Figure 7. At 20 s, a vehicle cuts in, and the host vehicle brakes immediately to avoid a rear-end collision. By contrast, at 40 s, the cut-in vehicle drives out of its position, and the intervehicle distance quickly increases. The proposed controller provides a greater engine torque in order for the host vehicle to keep up with the preceding vehicle. No surplus acceleration (which always leads to surplus braking) is generated in the entire process, thereby helping conserve energy. Figure 7 also shows that the acceleration of the host vehicle is in a reasonable range in both the cut-in and cut-out scenarios, thereby verifying that the proposed controller takes ride comfort into account.

## 5 Experimental results

The test platform, which is shown in Figure 8, consists of a host vehicle and two preceding vehicles. The host vehicle is a production SUV. One of the preceding vehicles is equipped with an AT, while the other is equipped with a manual transmission (MT). The host vehicle is equipped with a Mobileye camera, a millimeter-wave radar, a rapid prototyping-system MicroAutoBoxII (with 900 MHz clock frequency and PPC750 GL power PC processor), and an additional vehicle gateway. The Mobileye system recommends a target vehicle from the view of the camera. The speed of the target vehicle and the intervehicle distance are obtained through data fusion, where the original signals come from the Mobileye camera and the millimeter-wave radar. The additional vehicle gateway is used to manage the vehicle-to-sensor communication.

The software implementation process is summarized as follows: (i) Establish the proposed control scheme with MATLAB/Simulink; (ii) Transform the controller into real-time C source codes using the embedded coder; (iii) Download C source codes on the rapid prototyping-system MicroAutoBoxII; (iv) Monitor the signals and calibrate the controller gains online using the hardware management software ControlDesk. The actuators are the engine control unit and the electronic stability control system. The entire experiment is carried out under good open-road conditions (no rain, no wind). The system sampling time of the real-vehicle implementation is 0.01 s. Other important system parameters for the designed controller are listed in Table 1.

### 5.1 Performance of road-slope approximation method

To illustrate the accuracy of the proposed road-slope approximation method, experiments are performed on the host vehicle. The experimental results of the slope angle approximation are given in Figure 9. Test roads with uphill and downhill sections are chosen in the experiments, and the real slope angle is obtained

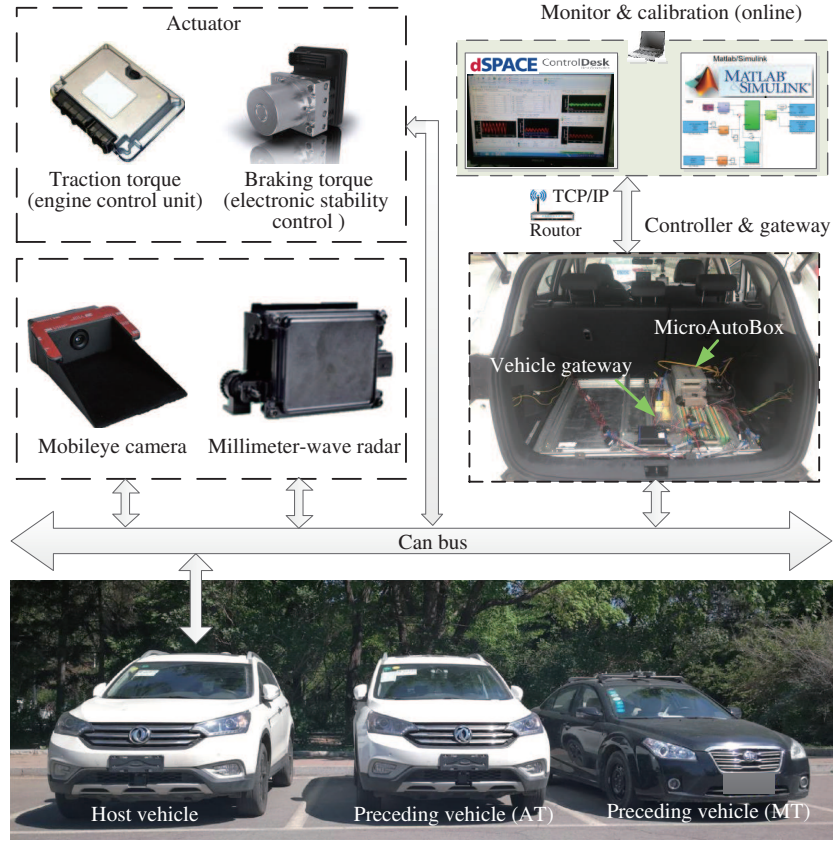


Figure 8 (Color online) Test platform.

Table 1 System parameters for controller design

Symbol	Description	Value	Unit
$m_v$	Vehicle mass	1700	kg
$C_D$	Aerodynamic drag coefficient	0.373	–
$A_a$	Frontal area	2.58	m <sup>2</sup>
$f$	Rolling resistance coefficient	0.011	–
$r_w$	Wheel radius	0.364	m
$d_0$	Intervehicle distance	3	m
$\tau$	Nominal time headway	2	s
$\tau_i$	Acceleration time constant	0.9	s
$q_{11}, q_{22}, q_{23}$	Weighting matrix $Q$	0.15, 0.73, 0.2	–
$r$	Weighting matrix $R$	1	–
$K_x(1), K_x(2), K_x(3)$	Controller gains for states	0.385, 0.922, –1.012	–
$K_d$	Controller gain for the disturbance	0.163	–

from a high-definition map. More details about the high-definition map can be found in [26]. The actual longitudinal acceleration is calculated from the differential of the velocity of the nondriven wheels, as shown in Figure 5. As seen in the bottom subfigure of Figure 9, the maximal absolute approximation error of this method is less than  $0.8^\circ$ . Its mean square error (MSE) is 0.09. Therefore, the proposed road-slope approximation method is accurate enough for acceleration tracking control. In addition, the solid-line box in Figure 9 indicates that the slope approximation method can also be used in braking conditions.

## 5.2 Car-following performance comparison

Comparison experiments are performed on the host vehicle and the AT preceding vehicle for different controllers. The AT preceding vehicle is controlled to track the same predefined mission profile, which is

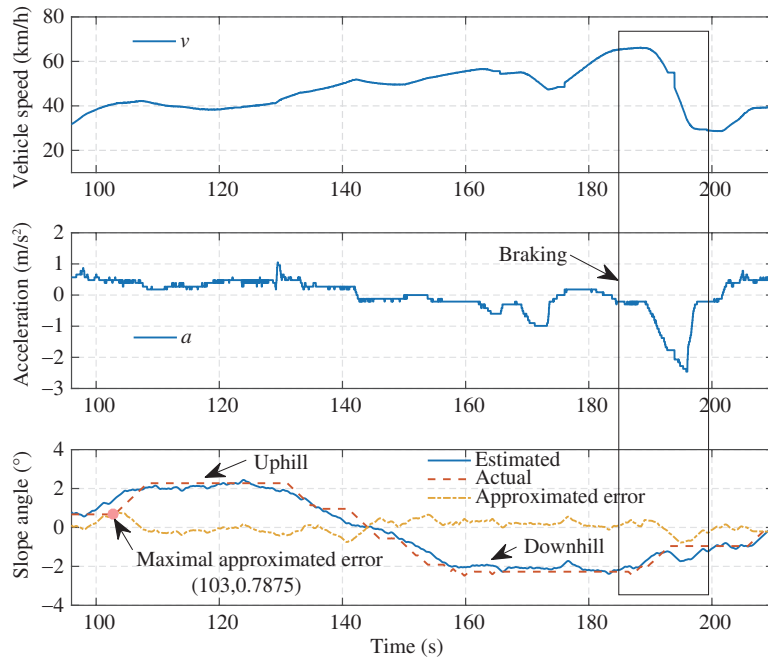


**Figure 9** (Color online) Experimental results of slope angle approximation.

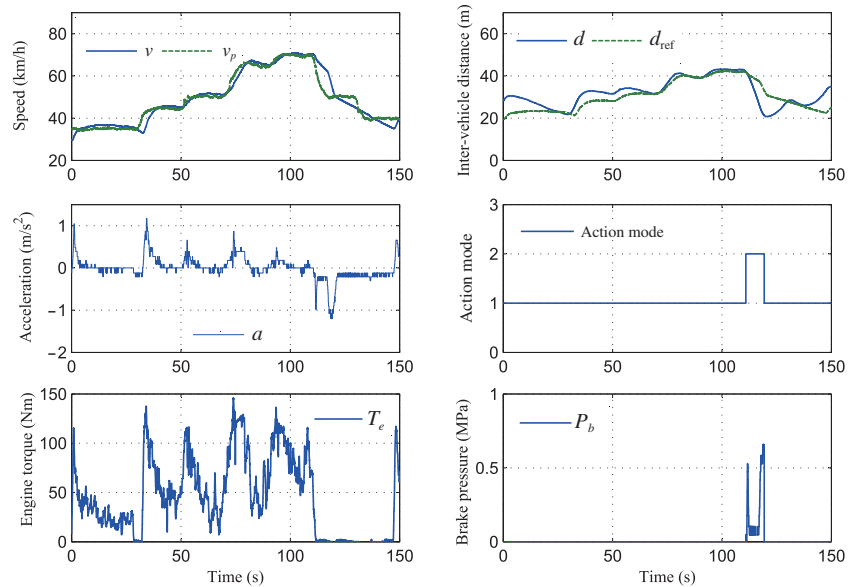


**Figure 10** (Color online) Experimental results of the proposed control scheme (action mode: 1-traction control; 2-brake control).

composed of the acceleration, constant speed, and deceleration. The host vehicle is separately controlled by the proposed controller, a factory-installed ACC, and a human driver to follow the preceding vehicle. The experimental results for these three controllers are shown in Figures 10–12, respectively.

The factory-installed ACC is developed to perfectly track the space policy. Although steady-state errors exist, the factory-installed ACC has better tracking performance. The proposed optimal controller is multiobjective and allows for a certain number of tracking errors to help reduce the number of braking operations. Judging from the braking operations of Figures 10 and 11, it can be seen that the overregulation of the proposed optimal controller is less than that of the factory-installed ACC, thereby improving vehicle comfort. Figures 10–12 show that compared with the factory-installed ACC, the control performance of the proposed control scheme is closer to the human driver. This result is mainly attributed to the fact that the proposed control scheme takes ride comfort into consideration. From this perspective, the proposed control scheme may be more easily accepted by the user than the factory-installed ACC.

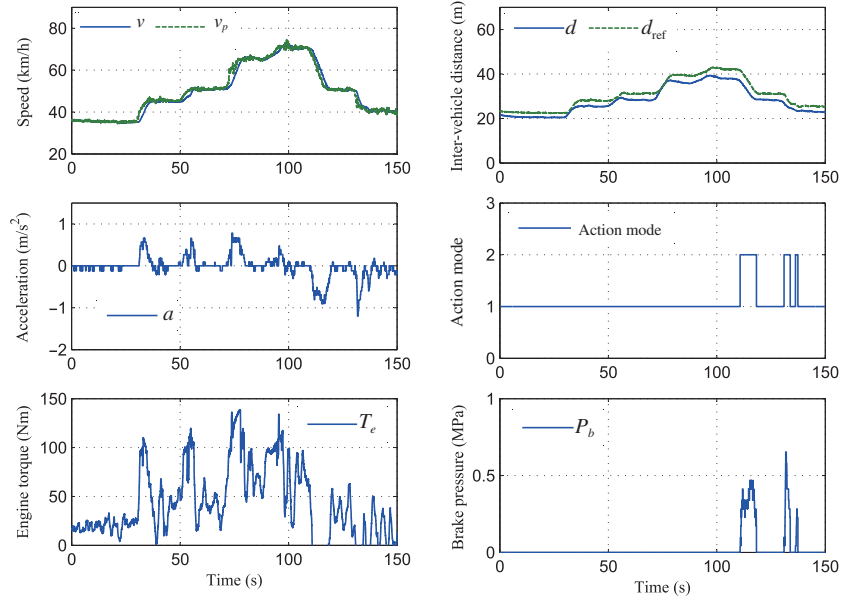


**Figure 11** (Color online) Experimental results of the factory-installed ACC (action mode: 1-traction control; 2-brake control).

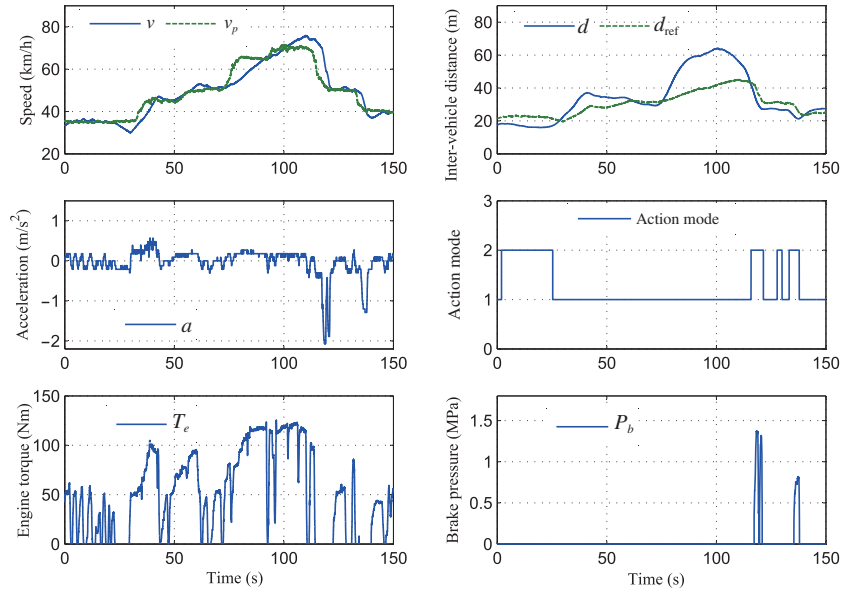


**Figure 12** (Color online) Experimental results of the human driver (action mode: 1-traction control; 2-brake control).

**Table 2** Performance comparison

Controller	Cost function value ( $\times 10^5$ )	MSE of the spacing error $\delta$	MSE of the relative speed $\varpi$
Proposed optimal controller	1.11	19.8	0.73
Factory-installed ACC	1.79	32.4	0.22
Human driver	4.41	79.5	1.36

To quantify the performance of the proposed control scheme for the car-following scenario, the cost function values and tracking errors of the three different controllers are compared in Table 2. The comparison results show that the MSE of the relative speed obtained by the proposed optimal controller is larger than that obtained by the factory-installed ACC. However, opposite results are obtained for the MSE of the spacing error and the cost function value. The performance indexes obtained by the human driver are classified as the worst.

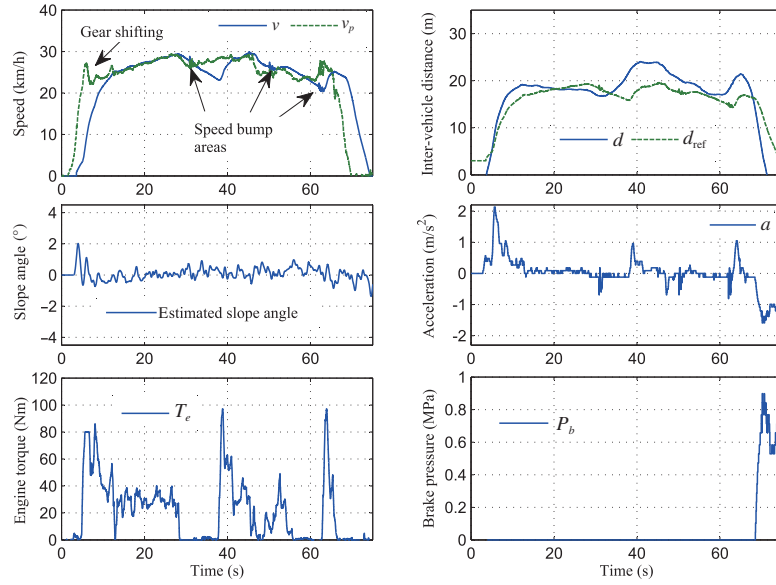


**Figure 13** (Color online) Control and slope approximation performance in low-speed conditions.

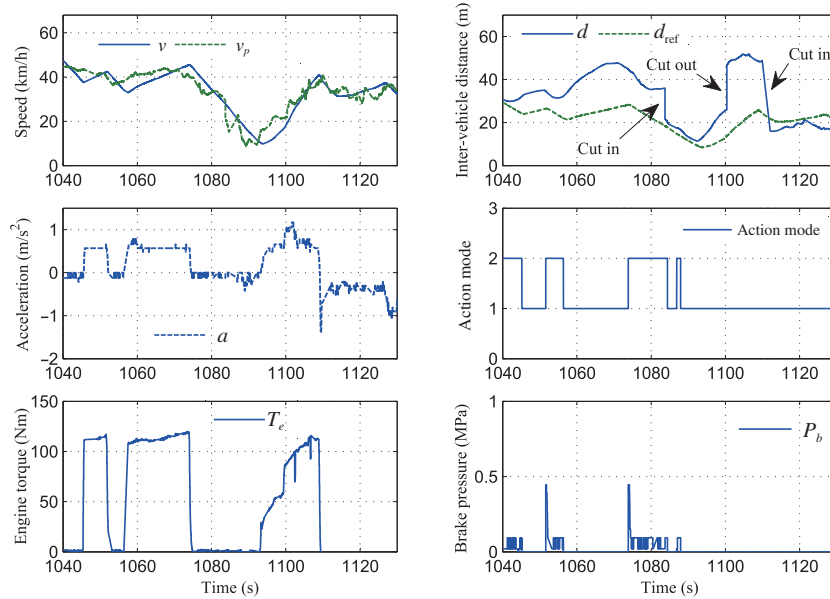


**Figure 14** (Color online) Experimental results of the proposed control scheme for cut-in and cut-out scenarios (action mode: 1-traction control; 2-brake control).

### 5.3 Robustness evaluation of the proposed control scheme

To evaluate the robustness of the proposed control scheme, experiments are performed in low-speed conditions. Some vehicle state signals, such as the vehicle speed and engine torque, are often accompanied by fluctuations under low-speed conditions, thereby making the vehicle control and road-slope approximation extremely difficult. Figure 13 shows the control and slope approximation performance of the proposed control scheme. In the experiments, some speed bumps are placed across the test road, and the preceding vehicle is selected as an MT vehicle with a power interruption during the gear-shifting process. As shown in Figure 13, the vehicles experience speed fluctuations when crossing the speed bumps. The proposed road-slope approximation method works effectively in this situation by introducing a rate limiter. In addition, it can be seen from Figures 9 and 13 that the road-slope approximation performance observed in medium-speed conditions is better than that observed in the low-speed conditions.

Finally, experiments are conducted for cut-in and cut-out scenarios. The experimental results are shown in Figure 14, in which the moments when the preceding vehicle cuts in and out are indicated.

From the engine torque and brake pressure of Figure 14, it can be seen that the proposed control scheme is robust against sudden changes in the intervehicle distance.

## 6 Conclusion

The study proposed the hierarchical design of optimal control to address multiobjective car-following problems. After establishing the vehicle longitudinal dynamics and the car-following model, the car-following controller was designed by using the LQR method. Afterward, both the feedforward-feedback method and the online road-slope approximation method were used to derive the acceleration-tracking controller. The performance of the proposed cruise control scheme was then evaluated by conducting simulations and real-vehicle experiments.

(i) The simulation results revealed that the car-following performance improved by introducing the acceleration of the preceding vehicle.

(ii) The experimental results showed that the proposed online road-slope approximation method provides a satisfactory road-slope approximation accuracy with a maximal absolute approximation error of less than  $0.8^\circ$ .

(iii) A comparison of the experimental results indicated that the car-following performance of the proposed optimal controller is better than that of a factory-installed ACC.

(iv) The robustness experiment results showed that the proposed control scheme is robust against low-speed, cut-in, and cut-out conditions.

The proposed controller can be applied easily to connected vehicles. For centralized-control connected vehicles, the proposed control scheme can provide an acceleration-tracking controller. For decentralized-control connected vehicles, the proposed control scheme can provide a car-following controller.

**Acknowledgements** This work was supported by China Automobile Industry Innovation and Development Joint Fund (Grant Nos. U1664257, U1864206), National Natural Science Foundation of China (Grant No. 61903153), and Postdoctoral Science Foundation of China (Grant No. 2018M641779). The authors would like to thank Yongjun YAN, Pengfei SUN, Liangchun ZHAO, Yuxiang ZHANG, Xin LI, and Ting QU for their help in the real-vehicle implementation of the proposed control scheme.

## References

- 1 Ganji B, Kouzani A Z, Khoo S Y, et al. Adaptive cruise control of a HEV using sliding mode control. *Expert Syst Appl*, 2014, 41: 607–615
- 2 Nilsson P, Hussien O, Balkan A, et al. Correct-by-construction adaptive cruise control: two approaches. *IEEE Trans Contr Syst Technol*, 2016, 24: 1294–1307
- 3 Yi K, Lee S, Kwon Y D. An investigation of intelligent cruise control laws for passenger vehicles. *Proc Inst Mech Eng Part D J Automobile Eng*, 2001, 215: 159–169
- 4 Li S E, Li K, Wang J. Economy-oriented vehicle adaptive cruise control with coordinating multiple objectives function. *Vehicle Syst Dyn*, 2013, 51: 1–17
- 5 Chu H, Guo L, Gao B, et al. Predictive cruise control using high-definition map and real vehicle implementation. *IEEE Trans Veh Technol*, 2018, 67: 11377–11389
- 6 Li S, Li K, Rajamani R, et al. Model predictive multi-objective vehicular adaptive cruise control. *IEEE Trans Contr Syst Technol*, 2011, 19: 556–566
- 7 Marzbanrad J, Moghaddam I T. Self-tuning control algorithm design for vehicle adaptive cruise control system through real-time estimation of vehicle parameters and road grade. *Vehicle Syst Dyn*, 2016, 54: 1291–1316
- 8 Moon S, Yi K. Human driving data-based design of a vehicle adaptive cruise control algorithm. *Vehicle Syst Dyn*, 2008, 46: 661–690
- 9 Darbha S, Konduri S, Pagilla P R. Benefits of V2V communication for autonomous and connected vehicles. *IEEE Trans Intell Transp Syst*, 2019, 20: 1954–1963
- 10 Wang Z, Wu G, Barth M J. A review on cooperative adaptive cruise control (CACC) systems: architectures, controls, and applications. In: *Proceedings of 2018 21st International Conference on Intelligent Transportation Systems (ITSC)*, 2018. 2884–2891
- 11 Cheng H T, Shan H, Zhuang W. Infotainment and road safety service support in vehicular networking: from a communication perspective. *Mech Syst Signal Process*, 2011, 25: 2020–2038
- 12 Li D Y, Liu M, Zhao F, et al. Challenges and countermeasures of interaction in autonomous vehicles. *Sci China Inf Sci*, 2019, 62: 050201
- 13 Li K, Tan H S, Misener J, et al. Digital map as a virtual sensor-dynamic road curve reconstruction for a curve speed assistant. *Veh Syst Dyn*, 2008, 46: 1141–1158
- 14 Yang D G, Jiang K, Zhao D, et al. Intelligent and connected vehicles: current status and future perspectives. *Sci China Tech Sci*, 2018, 61: 1446–1471
- 15 Jo K, Kim J, Sunwoo M. Real-time road-slope estimation based on integration of onboard sensors with GPS using an IMM/PDA filter. *IEEE Trans Intell Transp Syst*, 2013, 14: 1718–1732
- 16 Ohnishi H. A study on road slope estimation for automatic transmission control. *JSAE Rev*, 2000, 21: 235–240
- 17 Nourmohammadi H, Keighobadi J. Fuzzy adaptive integration scheme for low-cost SINS/GPS navigation system. *Mech Syst Signal Process*, 2018, 99: 434–449
- 18 Bae H S, Ryu J, Gerdes J C. Road grade and vehicle parameter estimation for longitudinal control using GPS. In: *Proceedings of the IEEE Conference on Intelligent Transportation Systems*, 2001. 25–29

- 19 Sun Y, Li L, Yan B, et al. A hybrid algorithm combining EKF and RLS in synchronous estimation of road grade and vehicle' mass for a hybrid electric bus. *Mech Syst Signal Process*, 2016, 68–69: 416–430
- 20 Vahidi A, Stefanopoulou A, Peng H. Recursive least squares with forgetting for online estimation of vehicle mass and road grade: theory and experiments. *Vehicle Syst Dyn*, 2005, 43: 31–55
- 21 Zhu M, Chen H, Xiong G. A model predictive speed tracking control approach for autonomous ground vehicles. *Mech Syst Signal Process*, 2017, 87: 138–152
- 22 Li L, Wang X, Song J. Fuel consumption optimization for smart hybrid electric vehicle during a car-following process. *Mech Syst Signal Process*, 2017, 87: 17–29
- 23 Darbha S, Konduri S, Pagilla P R. Benefits of V2V communication for autonomous and connected vehicles. *IEEE Trans Intell Transp Syst*, 2019, 20: 1954–1963
- 24 Ogata K. *Discrete-Time Control Systems*. Englewood Cliffs: Prentice Hall, 1995
- 25 Bryson A E, Ho Y C, Siouris G M. *Applied optimal control: optimization, estimation, and control*. *IEEE Trans Syst Man Cybern*, 1979, 9: 366–367
- 26 Chu H Q, Guo L L, Yan Y J, et al. Energy-efficient longitudinal driving strategy for intelligent vehicles on urban roads. *Sci China Inf Sci*, 2019, 62: 064201